Processing and Application of Ceramics 11 [2] (2017) 147–153
https://doi.org/10.2298/PAC1702147Z



# Phase evolution during heat treatment of amorphous calcium phosphate derived from fast nitrate synthesis

Zoltan Z. Zyman*, Anton V. Goncharenko, Dmytro V. Rokhmistrov

*Physics of Solids Department, V.N. Karazin Kharkiv National University, 4 Svoboda Sq., Kharkiv 61022, Ukraine*

Received 28 December 2017; Received in revised form 20 April 2017; Accepted 29 May 2017

## Abstract

*The phase evolution in amorphous calcium phosphate (ACP, with a Ca/P ratio of 1 : 1), derived from the fast nitrate synthesis using different conditions, was studied in temperature range 20–980 °C. ACP crystallized within 600–700 °C and the phase composition depended on the synthesis duration. It was firstly revealed that for an extremely short synthesis (1 min) two metastable phases α′-CPP and α′-TCP of the high-temperature calcium pyrophosphate α-CPP and tricalcium phosphate α-TCP were crystallized. For a longer synthesis (5 min), α′-CPP and minor β-CPP crystallized. The metastable phases gradually transformed to stable polymorphs β-CPP and β-TCP above 800 °C, and a biphasic mixture β-CPP/β-TCP or β-CPP formed at 980 °C. The crystallization of the metastable phases was attributed to the Ostwald step rule. A mechanism for the formation of TCP (Ca/P = 1.5) from ACP (Ca/P = 1) was proposed. The prepared powders of β-CPP/β-TCP, β-CPP or initial ACP were fine-grained and would have enhanced sinterability. Contribution to the densification was demonstrated due to the thermal transformation of the metastable polymorphs into stable phases having higher densities.*

***Keywords:*** *amorphous calcium phosphates, crystallization, structural characterization, metastable phases*

## I. Introduction

Porous $\beta$-calcium pyrophosphate ($\beta$-Ca2P2O7, $\beta$-CPP) has been recently presented as a graft material because it is bioactive, more completely incorporated and more rapidly resorbable in bone than porous HA [1]. There are three CPP polymorphs: $\gamma$-CPP exists in a relatively low temperature range, $\beta$-CPP at mediate temperatures, and $\alpha$-CPP is the high-temperature polymorph (above 1200 °C) [2,3]. $\alpha$-CPP is typically prepared by a solid-state route [1,3]. Maciejewski *et al.* [4] demonstrated that $\alpha$-CPP nanopowder can also be obtained from ACP with a Ca/P ratio < 1.5 at a mediate temperature (in this study this metastable $\alpha$-CPP is designated as $\alpha'$-CPP). However, the ACP was prepared by the flame spray synthesis, which is rather complicated and has a low yield.

High-temperature $\alpha$-tricalcium phosphate ($\alpha$-TCP) has become growing interest as a component for CP cements and ceramics [5,6]. $\alpha$-TCP is stable above 1125 °C and is produced by a high-temperature process. A nanosized $\alpha$-TCP powder was prepared by firing amorphous calcium phosphate (ACP) precipitate with a Ca/P ratio of 1.5 in the range of 500–700 °C [6–8]. $\alpha$-TCP crystallized at these mediate temperatures is also metastable (designated as $\alpha'$-TCP in this study).

Both $\alpha$-CPP and $\alpha$-TCP are typically produced by a high-temperature process. A powder from the process consists of large particles with high crystallinity, which significantly reduces its bioactivity compared to a nanocrystalline one [9–12]. It was recently observed that fine-grained $\alpha'$- and $\beta$-CPPs and small amount of $\beta$-TCP can be formed from ACP powder with a Ca/P ratio of 1 : 1 using a fast variation of the nitrate synthesis upon heating above 800 °C [13]. $\beta$-TCP is well known due to excellent bioactivity [12], so its presence may improve the biological performance of the CPPs. The formation of $\beta$-TCP was unexpected because the Ca/P ratio for $\beta$-TCP should be 1.5, and this ratio in the mother solution was only 1 : 1. It was assumed that the $\beta$-TCP formation resulted from the reaction of residual calcium from calcium nitrate (stock salt) with CPP. Formation of calcium phosphate (CP) with a higher Ca/P ratio than the given in mother solution (for Ca/P < 1)

* Corresponding author: tel: +38 057 707 56 84,
e-mail: *intercom@univer.kharkov.ua*

was also observed earlier [14] under the conditions similar to those in the study [13]. However, no explanation was proposed [14] for this effect.

The aim of this study was to prepare fine powders based on CPP and TCP including their metastable polymorphs, and to examine thermal phase evolution in the powders. The idea was also to get more data on the mechanism of TCP formation in the powders derived from the fast nitrate syntheses under Ca/P of 1 : 1, proposed recently in literature [13].

## II. Materials and methods

Amorphous calcium phosphate was prepared using the fast nitrate synthesis [15,16]. A 0.5 M solution of calcium nitrate tetrahydrate $Ca(NO_3)_2 \cdot 4\,H_2O$ was rapidly added into a 0.5 M solution of ammonium phosphate dibasic $(NH_4)_2HPO_4$ (both in distilled water). Each of the solutions was preliminary adjusted to pH between 10 and 11 with an ammonium hydroxide solution $NH_4OH$ and cooled down to 5 °C. Because Ca/P ratio in the resulted mother solution was 1 : 1, the following synthesis reaction, with calcium hydrophosphate and ammonium nitrate as by-product, was expected:

$$Ca(NO_3)_2 + (NH_4)_2HPO_4 \longrightarrow CaHPO_4 + 2\,NH_4NO_3$$

Three kinds of powders were prepared. For the powder P1, the reaction time after mixing the solutions was 5 min. To stop the reaction, the mother liquor with precipitate was poured out into a cooled crucible and immediately put into a freezer. After freezing for 2 days at −25 °C, the formed ice cake was slowly warmed up to about 1 °C, and the appeared liquid was continuously removed by blotting paper. The resulted wet mass was put back into the freezer and kept there until transformed to a dry friable powder. The powder P2 was prepared in the same way as the powder P1, but the formed precipitate was aged for about 2 years in the freezer. To get more unreacted calcium compared to that in the powder P1, the powder P3 was processed similarly to the powder P1 except for the synthesis time, which was shortened about 5 times and not exceeded 1 min.

The powders were examined in the as-prepared state and after heating (5 °C/min) in air to different temperatures in the range of 20–980 °C in a muffle furnace. The heated samples were removed from the furnace and allowed to cool to a room temperature. The as-prepared and heated samples were characterized by X-ray powder diffraction, XRD (DRON-2, USSR and Philips APDW 40C diffractometers; $CuK_\alpha$ radiation, 0.154 nm), combined thermogravimetry and differential thermal analysis, TG-DTA (Q-Derivatograph, Hungary, 5 K/min, in air), infrared spectrometry, IR (Perkin-Elmer 1720X and Specord 751, Germany; KBr-pellet technique). Phase composition and crystal size were determined by the Rietweld refinement using the program package TOPAS 4.2 from Bruker. The morphology was observed in a scanning electron microscope (ESEM Quanta 400 FEG instrument, FEI, gold sputtered samples), and the Ca/P ratio was estimated by EDX spectroscopy (Genesis 4000, SUTW-Si detector).

## III. Results

The TG curve of the powder P1 showed a mass loss of 27.5 wt.% (Fig. 1a, curve 1). The corresponding DTG track displayed intense mass losses at about 100 °C and 620 °C (Fig. 1b, curve 1′). A number of weak peaks at

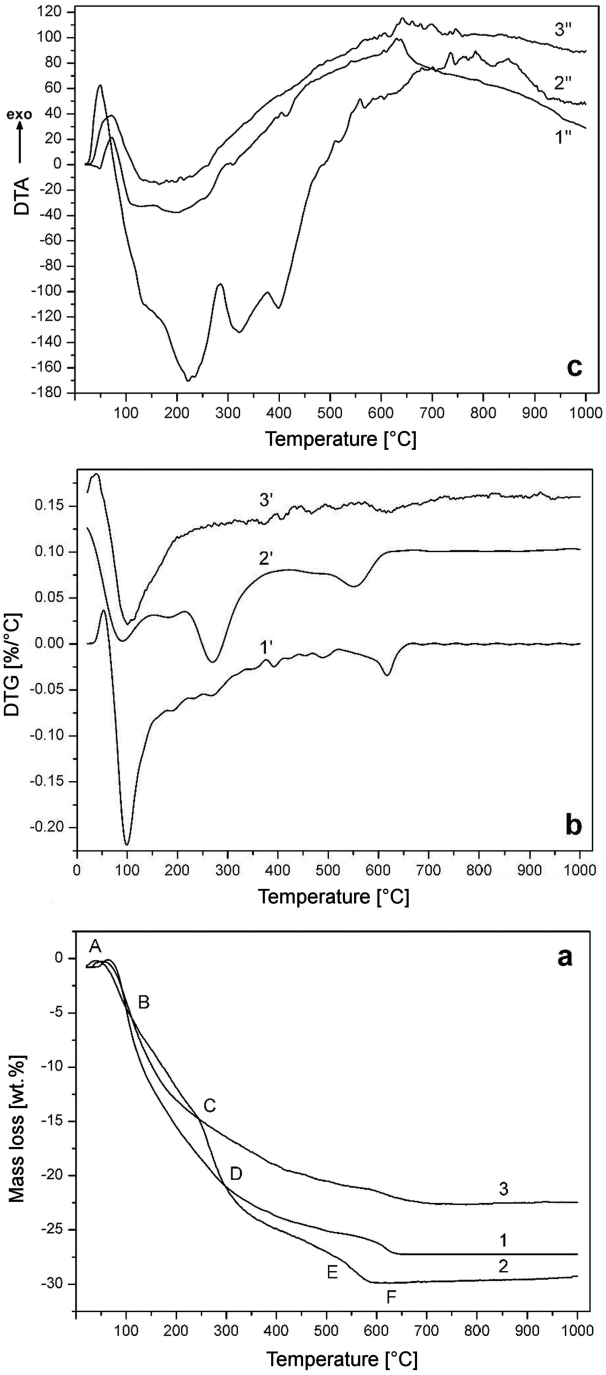


**Figure 1. TG (a), DTG (b) and DTA (c) curves for powders P1 (1, 1′, 1″), P2 (2, 2′, 2′) and P3 (3, 3′, 3′) Note: in Fig. 1b, curves 2′ and 3′ were plotted in the same scale as curve 1′ and shifted along the ordinate to avoid superimposition**

about 180, 230, 270, 320, 400 and 490 °C were identified and possibly small mass losses were also presented. Endothermal minima in the DTA curve seem to be positioned at these temperatures (Fig. 1c, curve 1″). However, they were overlapped, and this made difficult unambiguous identification. An exothermal peak with a top at about 630 °C was also present.

To investigate the initial stages of the synthesis, unwashed precipitates (typically used for processing the powder P1 and containing much adsorbed water) were subjected to a prolonged ageing in the freezer. The TG curve of the powder P2 from the precipitate aged for 2 years had a sectional structure (Fig. 1, curve 2). The curve was tentatively divided into a few sections: AB (20–120 °C), BC (120–240 °C), CD (240–290 °C), DE (290–530 °C) and EF (530–650 °C). Increased rates of mass loss were observed in these temperature ranges (Fig. 1b, curve 2′). The endothermal minima became distinctly developed (Fig. 1c, curve 2″). However, the exothermal peak was extended and shifted toward lower temperature range (500–600 °C).

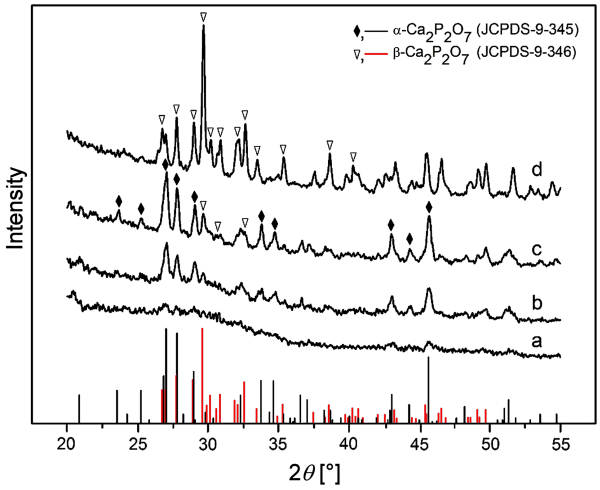


**Figure 2. XRD patterns of powder P1 heated to 600 °C (a), 720 °C (b), 800 °C (c) and 980 °C (d)**

The as-prepared powder P1 was X-ray amorphous, and the amorphous state was observed in the powder heated up to 600 °C (Fig. 2a). First weak peaks appeared above 600 °C, became stronger at 630 °C, and somewhat sharper up to 720 °C. Two phases, $\alpha'$-CPP and $\beta$-CPP, were identified (Fig. 2b). These data were well consistent with the exothermal peak at 630 °C (Fig. 1c, curve 1″) which thus was caused by the crystallization of the phases. The relative amount of $\alpha'$-CPP was slightly increased upon heating to a higher temperature, and reached a maximum at 800 °C (Fig. 2c); according to the Rietveld refinement, the powder consisted of 69 wt.% $\alpha'$-CPP and 31 wt.% $\beta$-CPP. The $\alpha'$-CPP/$\beta$-CPP ratio gradually decreased at higher temperature, and the powder heated at 980 °C for 15 min was solely $\beta$-CPP (Fig. 2d; minor amount of $\alpha'$-CPP was present for a shorter dwell time at this temperature).

Thermal phase evolution in the powder P2 was different in the low-temperature range in comparison to the sample P1. In the XRD pattern of the as-prepared powder P2, the typical diffusion peak of ACP at 30° 2$\theta$ [8,16,17] (observed also for the powder P1) was shifted to 29° 2$\theta$ and a new relatively narrow peak appeared at about 22° 2$\theta$. Also, sharp diffraction peaks of $NH_4NO_3$ were present (Fig. 3a). The distinction in structure, detected by the XRD pattern, affected the thermal behaviour of the powder P2. Compared to the powder P1, the crystallization started at a markedly lower temperature, i.e. 400 °C, instead of above 600 °C. The crystallized phases were $\gamma$-CPP with small amount of $\beta$-CPP instead of $\alpha'$-CPP and $\beta$-CPP (Figs. 3b and 2b). As the heating temperature was increased, $\gamma$-CPP gradually transformed to $\beta$-CPP. Weak peaks of $\alpha'$-CPP appeared above 500 °C and became clearly discernible at 600 °C (Fig. 3c). Phase evolution in the powder P2 at higher temperatures was similar to that in the powder P1. A biphasic mixture of $\alpha'$-CPP and $\beta$-CPP was formed at 800 °C, and a single-phase powder of $\beta$-CPP resulted after heating to 980 °C (Fig. 3d). Hence, the weak separated exothermal peaks in the DTA track for the powder P2 (Fig. 1c, curve 2″) were associated with the crystallization of metastable $\alpha'$-CPP and its subsequent gradual transformation into thermodynamically stable $\beta$-CPP.

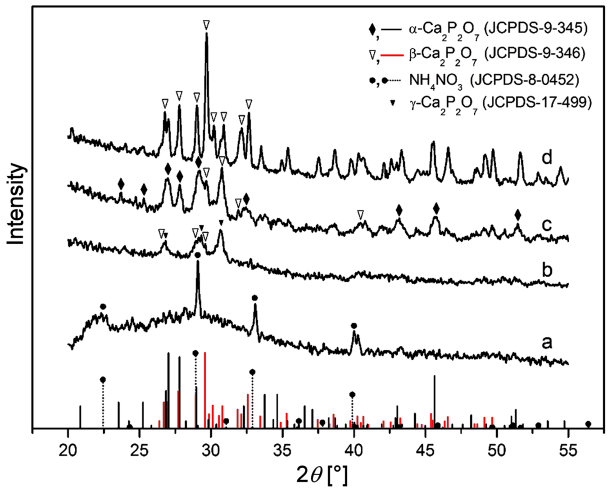


**Figure 3. XRD patterns of powder P2 after two-year ageing (a) and heating to 400 °C (b), 600 °C (c) and 980 °C (d)**

Contrary to the powder P1 and particularly to the powder P2, the TG curve for the powder P3 was mainly smooth (Fig. 1a, curve 3). DTG also revealed only one significant mass loss at about 100 °C and poorly discernible peaks at higher temperatures (Fig. 1b, curve 3′). The DTA examination showed a relatively weak and unresolved endothermal minimum in the range of 100–300 °C and an exothermal event within 630–760 °C (Fig. 1c, curve 3″).

The as-prepared powder P3 was X-ray amorphous (Fig. 4a) and retained this state up to 600 °C. In the patterns of the powder heated to a higher temperature, first diffraction peaks appeared at 640 °C (Fig.

**Table 1. Thermal phase evolution in the powders**

| Sample | Temperature [°C] | | | | | |
|---|---|---|---|---|---|---|
| | 20 | 400 | 600 | 720 | 800 | 980 |
| Powder 1 | ACP | ACP | ACP | $\alpha'$-CPP<br>$\beta$-CPP | $\alpha'$-CPP (69 wt.%)<br>$\beta$-CPP (31 wt.%) | $\beta$-CPP |
| Powder 2 | ACP<br>$NH_4NO_3$ | $\gamma$-CPP<br>$\beta$-CPP, ACP | $\alpha'$-CPP<br>$\beta$-CPP | $\alpha'$-CPP<br>$\beta$-CPP | $\alpha'$-CPP<br>$\beta$-CPP | $\beta$-CPP |
| Powder 3 | ACP | ACP | ACP | $\alpha'$-CPP, $\beta$-CPP,<br>$\alpha'$-TCP, ACP | $\alpha'$-CPP, $\beta$-CPP,<br>$\alpha'$-TCP | $\beta$-CPP,<br>$\beta$-TCP |

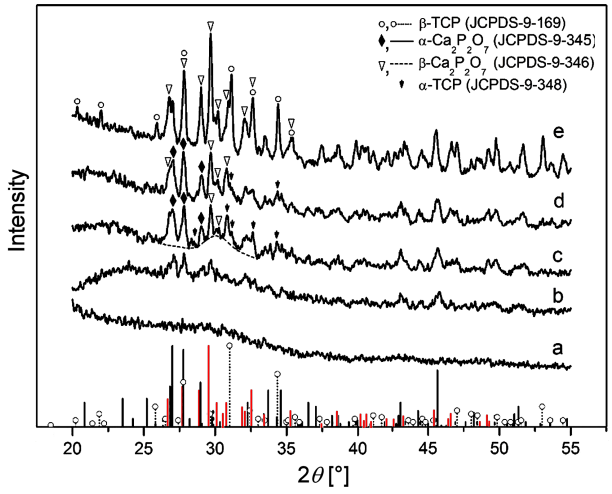


**Figure 4. XRD patterns of powder P3 as-prepared (a), and heated to 640 °C (b), 720 °C (c), 800 °C (d) and 980 °C (e)**

4b). They strengthened at 680 °C and became discernible at 720 °C. These data were in accordance with the extended exothermal peak in the range of 630–760 °C (Fig. 1c, curve 3″). Three phases were identified, namely $\alpha'$-CPP, $\beta$-CPP and $\alpha'$-TCP. Also, some residual ACP was present giving a hump under peaks (shown by a broken line in Fig. 4c). The residual ACP crystallized at higher temperature, and the powder upon heating to 800 °C was a triphasic mixture of $\alpha'$-CPP, $\beta$-CPP and $\alpha'$-TCP (Fig. 4d). During heating above 800 °C, $\alpha'$-CPP gradually transformed into $\beta$-CPP and $\alpha'$-TCP into $\beta$-TCP, i.e. the two metastable phases transformed into stable polymorphs at these temperatures. Finally, the powder P3 upon heating to 980 °C was a biphasic mixture of $\beta$-CPP and $\beta$-TCP (Fig. 4e). For the convenience of further discussion, the thermal phase evolution in the powders is presented in the Table 1.

Because the powders P1 and P3 were primarily intended for ceramics processing, their sintering ability was assessed. The particles in the powder P3 were in rounded form and nanometer size at 600 °C right before crystallization, became somewhat smaller in size with spherical-like morphology after the crystallization at 630–700 °C, and clearly started joining and growing above 700 °C (Fig. 5a–c). By the Rietveld refinement, the average crystallite sizes for phases in the powder were in the nanorange (74–93 nm) at 800 °C, somewhat higher (120–160 nm) at 900 °C, and of submicron sizes at 980 °C (Fig. 5d). The powder P1 had similar trends in the sizes after the same heating treatment. The average Ca/P ratios were 1.04±0.05 in the powder P1 and 1.24±0.25 in the powder P3 after heating the powders to 900 and 980 °C, respectively (Fig. 5d,e).

## IV. Discussion

The processes during heating of the powders P1 and P2 may be explained as follows. The abrupt mass loss and the related endothermal minimum (section AB) were caused by the liberation of adsorbed water (Fig. 1) [17]. The medium mass loss and the overlapped endothermal minimum at about 180 °C (section BC) resulted from the desorption of structural water [18]. The mass loss and the endothermal minimum in the range of 240–290 °C (section CD) were due to the release of gaseous products from the decomposition of by-product $NH_4NO_3$ in this range [16,19]. The mass loss and the broad endothermal minimum in the range of 300–500 °C (section DE) were relatively complicated. The typical thermal phase transition for crystalline monetite can be represented as follows [20]:

$$CaHPO_4 \longrightarrow (475\ ^\circ C) \longrightarrow \gamma\text{–CPP} \longrightarrow (600\ ^\circ C) \longrightarrow \beta\text{–CPP} \longrightarrow (>1200\ ^\circ C) \longrightarrow \alpha\text{–CPP}$$

However, the minimum at about 320 °C was attributed to the condensation reaction:

$$2\,CaHPO_4 \longrightarrow Ca_2P_2O_7 + H_2O\uparrow$$

because the reaction is shifted to a lower temperature at about 300 °C in ACP [21]. The origins of the minimum at 400 °C, the broad exothermal peak near 550 °C (section EF) and weak separated exothermal peaks in the range of 650–900 °C are discussed in the following.

According to the TG-DTA the absence of diffraction peaks for the by-product in the patterns of the as-prepared powders P1 and P3 was because $NH_4NO_3$ is a highly hygroscopic (and soluble) salt [19]. According to the TG-DTA examination (Fig. 1, curve 1), the mass loss before 240 °C of about 18 wt.% was associated with desorption of water. The by-product was amorphous because it was hydrolyzed. Long-term ageing of the powder P2 was simultaneously a freeze drying process and, as a result, $NH_4NO_3$ lost absorbed water and crystallized. The shift of the main XRD diffusion peak and the appearance of another one (Fig. 3a), most likely, were

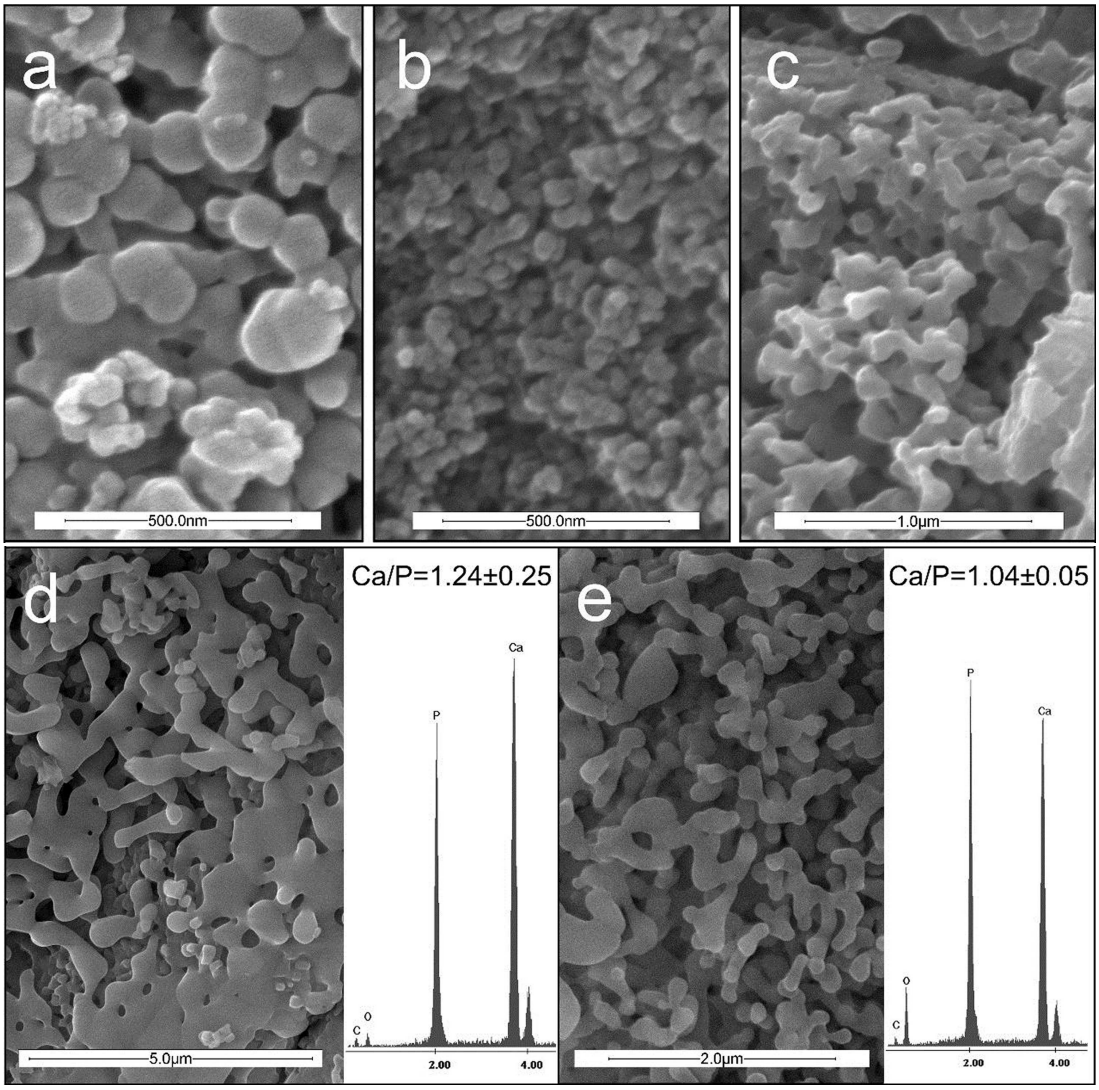


**Figure 5. SEM and EDX examinations of powder P3 after heating to 600 °C (a), 640 °C (b), 720 °C (c), 980 °C (d) and powder P1 after heating to 900 °C (e)**

also caused by the loss of water. The lowest mass loss and desorption speed for the powder P2 in the range of 20–200 °C compared to those of the powders P1 and P3 (Fig. 1a,b) confirmed this conclusion.

Because the main exothermal peak for the powder P2 was positioned in the temperature range EF (Fig. 1a,c), one can deduce that the metastable $\alpha'$-CPP phase crystallized from an amorphous part of the powder. $\gamma$-CPP resulted from another part of the powder P2 which crystallized during ageing. The condensation of $CaHPO_4$ into $\gamma$-CPP above 300 °C, and the transformation of $\gamma$-CPP into $\beta$-CPP at higher temperature are known for crystalline monetite [20,22]. Hence, the broad endothermal minimum with tops at above 300 and 400 °C was due to these processes (Fig. 1c, curve 2″). This is in agreement with the XRD data. Though the XRD pattern of the powder P2 displayed allegedly an amorphous substance, the shift of the main peak to a lower diffraction angle from the typical position for an ACP suggested that a crystalline part was present (Figs. 3a and 2a). A similar shift (to the opposite angle direction) caused by the partial crystallization of ACP (into HA) was observed earlier [23].

Another approach also leads to the above conclusion. It was found that ACP with Ca/P = 1 crystallized into the high-temperature polymorph $\alpha$-CPP [4]. However, the crystallization happened at 600–700 °C, and the polymorph was specified as metastable at these mediate temperatures. The main phase crystallized in the powder P1 at similar temperatures was also $\alpha$-CPP (designated as $\alpha'$-CPP in this study). Therefore, we assumed that the major part of the powder P1 was amorphous. The thermal condensation of crystalline $CaHPO_4$ at 400–600 °C results in the $\gamma$-CPP polymorph that gradually transforms into $\beta$-CPP polymorph at increasing temperatures [20] (see also the phase sequence in the powder P2, Figs. 3b,c) [19]. Since the secondary phase in the crystallized powder P1 was $\beta$-CPP, we assumed that the minor part of the as-prepared powder P1 was cryptocrystalline CP with Ca/P = 1 which did not reveal itself in the XRD pattern because of extremely tiny nanocrystals and so the powder P1 was XRD-amorphous.

Based on these data and assumptions, the thermal phase sequences in the powders P1–P3 may be explained as follows. In case of the short (5 min) synthesis (the powder P1), as the temperature was increased, the metastable $\alpha'$-CPP polymorph gradually transformed into $\beta$-CPP, and finally the thermodynamically stable $\beta$-CPP polymorph was formed. In case of the aged powder (the sample P2), the main phase formed and recrystallized from the tiny nanocrystals at above 400 °C was $\gamma$-CPP. In accordance with the typical phase sequence for monetite, $\gamma$-CPP transformed to $\beta$-CPP as the temperature was increased. However, a small amount of ACP remained in the aged powder P2. This residual ACP crystallized at about 600 °C into $\alpha'$-CPP, and the further thermal phase evolution was similar to that in the powder P1 (Table 1).

The thermally activated processes before crystallization, observed in the powders P1 and P2, were poorly developed in the powder P3. This implied that only small amounts of reaction products were present in the powder P3 because the synthesis was very short and not exceeded 1 min. Also, the shift of the crystallization range to higher temperatures suggested that the phase composition has to be different. Actually, beside some residual ACP, $\alpha'$-CPP and $\beta$-CPP, a noticeable amount of $\alpha'$-TCP was detected at 720 °C (Table 1). During crystallization of the residual ACP in the range of 720–800 °C, intensities of $\alpha'$-CPP maxima mainly increased. The crystallization of metastable $\alpha'$-CPP from ACP may be associated with the Ostwald step rule [24]. If metastable $\alpha'$-TCP also crystallized from ACP due to this rule, one should accept that areas enriched with calcium were present in ACP. It is quite likely because the synthesis was ultra-short, and some unreacted calcium form or as $Ca(NO_3)_2$ were present in the precipitate [13]. Residual calcium nitrate decomposes into CaO at about 480 °C in ACP from an early stage of precipitation [16]. Hence, in the areas where appropriate amounts of CaO and CPP appeared, TCP formed according to the reaction [22]:

$$CaO + Ca_2P_2O_7 \longrightarrow Ca_3(PO_4)_2$$

It is hardly believed that $\alpha'$-TCP crystallized from ACP with Ca/P = 1.5 formed during the wet synthesis (and consisted of e.g. Posner clusters). In this case, crystallization of CP phases with Ca/P < 1 would be also expected because the Ca/P ratio in the mother solution was only 1 : 1. However, such phases were not observed. Consequently, the metastable polymorphs $\alpha'$-CPP crystallized from ACP with Ca/P = 1 and $\alpha'$-TCP from ACP with Ca/P = 1.5 resulted from a reaction of the former and a calcium residue (i.e. as CaO).

The average Ca/P ratio in the powder P1 after heating to 900 °C was 1.04±0.05. The ratio is somewhat higher than in the mother solution (Ca/P = 1.0). This implies that the ratio may result from the presence of a minor amount of residual calcium in the powder. However the ratio difference was rather small to come to this conclusion unambiguously. The Ca/P ratios in different areas of the powder P3 after the high-temperature treatment were as 0.91, 0.95, 1.24, 1.48 and 1.64 with an average ratio 1.24±0.25. The lower deviations from the average value are close to the ratio in the mother solution, while the higher deviations cannot be attributed to the experimental error (±0.02). We associate the higher ratios with the presence of TCPs in the powder P3 in full accordance with the XRD data (Fig. 4e).

Sintering behaviour of the elaborated powders has not been studied yet. However, some relevant results on sintering of a CP nanocrystalline powder with Ca/P < 1.67 may be taken into consideration [25,26]. Nanocrystals in the powder joined by coalescence above 500 °C and started sintering above 700 °C. The coalescence stage led to a considerable reduction in the specific surface area (SSA) and, consequently, in subsequent sintering activity of the particles. This stage should be much shorter for the elaborated powders because the ACP crystallization was completed in the range of 720–800 °C (Figs. 2c and 4c). Diffusion phenomena start developing in this range [26], so the newly formed nanocrystals with high SSA may start sintering immediately after the appearance. Also, metastable $\alpha'$-CPP and $\alpha'$-TCP, resulted from the crystallization, transformed into the stable polymorphs above 800 °C. The latter, $\beta$-CPP and $\beta$-TCP, have a higher density than the related high-temperature (or metastable) polymorphs [19,27]. Both these peculiarities may contribute to the densification.

## V. Conclusions

The phase evolution in ACP derived from the fast nitrate synthesis (Ca/P ratio of 1 : 1), using different conditions, was studied in temperature range 20–980 °C. ACP crystallized at 600–700 °C. In case of a 5 min synthesis, ACP crystallized at 600–700 °C and the phase evolution from metastable high-temperature calcium pyrophosphate $\alpha'$-CPP after the ACP crystallization to stable $\beta$-CPP at 980 °C was observed. However, for a shorter synthesis of 1 min, metastable high-temperature tricalcium phosphate $\alpha'$-TCP emerged additionally to $\alpha'$-CPP after the crystallization. Upon the transformation of the metastable phase to the stable polymorph above 800 °C, a biphasic mixture of $\beta$-CPP and $\beta$-TCP formed at 980 °C.

The crystallization of the high temperature polymorphs $\alpha$-CPP and $\alpha$-TCP as metastable phases from ACP at mediate temperatures was attributed to the Ostwald step rule. The unexpected formation of TCP (Ca/P = 1.5) from ACP (given Ca/P ratio of 1 : 1) was associated with the reaction of CPP with residual calcium (most likely, as CaO) from the stock salt because of extremely short synthesis. It is suggested, that this may be also the formation mechanism for higher Ca/P ratios, than the given ones in mother solutions, in ACPs

derived from the syntheses under similar conditions by other authors.

The elaborated final powders consisted of one-phase $\beta$-CPP or of a mixture of $\beta$-CPP with $\beta$-TCP. They were nano- and submicrocrystalline contrary to those microcrystalline typically obtained from solid-phase syntheses. It is expected that the powders, as well as initial ACP, should have high sinterability due to their fine size. Besides, the densification of the powders has to be additionally intensified due to the thermal transformation of the metastable phases into their stable polymorphs having higher densities.

**Acknowledgements:** The authors gratefully acknowledge Dr. O. Prymak for the Rietveld refinements and Dr. K. Loza for assistance in SEM observations (University of Duisburg-Essen, Germany).

## References

1. J.H. Lee, D.H. Lee, H.S. Ryu, D.S. Chang, K.S. Hong, C.K. Lee, "Porous beta-calcium pyrophosphate as a bone graft substitute in a canine bone defect model", *Key Eng. Mater.*, **240–242** (2003) 399–402.
2. B.C. Cornilsen, R.A. Sr. Condrate, "The vibrational spectra of $\beta$-$Ca_2P_2O_7$ and $\gamma$-$Ca_2P_2O_7$", *Inorg. Nucl. Chem.*, **41** (1979) 602–605.
3. B.C. Cornilsen, R.A. Sr. Condrate, "The vibrational spectra of $\alpha$-alkaline earth pyrophosphates", *J. Solid State Chem.*, **23** (1978) 375–382.
4. M. Maciejewski, T.J. Brunner, S.F. Loher, W.J. Stark, A. Baiker, "Phase transition in amorphous calcium phosphates with different Ca/P ratios", *Thermochim. Acta*, **468** (2008) 75–80.
5. G. Cicek, E.A. Aksoy, C. Durucan, N. Hasirci, "Alpha-tricalcium phosphate ($\alpha$-TCP): Solid state synthesis from different calcium precursors and the hydraulic reactivity", *J. Mater. Sci: Mater. Med.*, **22** (2011) 809–817.
6. Y. Li, W. Weng, K.C. Tam, "Novel highly biodegradable biphasic tricalcium phosphates composed of $\alpha$-tricalcium phosphate and $\beta$-tricalcium phosphate", *Acta Biomater.*, **3** (2007) 251–254.
7. E.D. Eanes, "Thermochemical studies on amorphous calcium phosphate", *Calc. Tiss. Res.*, **5** (1970) 133–145.
8. T. Kanazawa, T. Umegaki, N. Uchiyama, "Thermal crystallization of amorphous calcium phosphate to $\alpha$-tricalcium phosphate", *J. Chem. Tech. Biotechnol.*, **32** (1982) 399–406.
9. R.G. Carrodequas, S. De Aza, "$\alpha$-tricalcium phosphate: Synthesis, properties and biomedical applications", *Acta Biomater.*, **7** (2011) 3536–3546.
10. M. Bohner, "Reactivity of calcium phosphate cements", *J. Mater. Chem.*, **17** (2007) 3980–3986.
11. C.L. Camire, U. Gbureck, W. Hirsiger, M. Bohner, "Correlating crystallinity and reactivity in an $\alpha$-tricalcium phosphate", *Biomaterials*, **26** (2005) 2787–2794.
12. R.Z. LeGeros, "Biodegradation and bioresorption of calcium phosphate ceramics", *Clin. Mater.*, **14** (1993) 65–88.
13. Z. Zyman, M. Epple, A. Goncharenko, D. Rokhmistrov, O. Prymak, K. Loza, "Peculiarities in thermal evolution of precipitated amorphous calcium phosphates with an initial Ca/P ratio of 1:1", *J. Mater. Sci.:Mater. Med.*, **28** (2017) 52–58.
14. Y. Li, W. Weng, "In vitro synthesis and characterization of amorphous calcium phosphates with various Ca/P atomic ratios", *J. Mater. Sci.: Mater. Med.*, **18** (2007) 2330–2308.
15. E. Hayek, W. Stadlmann, "Preparation of pure hydroxyapatite for adsorption uses", *Angew. Chem. Int. Ed.*, **67** (1955) 327–338.
16. Z.Z. Zyman, D.V. Rokhmistrov, V.I. Glushko, "Structural and compositional features of amorphous calcium phosphate at the early stage of precipitation", *J. Mater. Sci.: Mater. Med.*, **21** (2010) 123–130.
17. J.M. Sedlak, R.A. Beebe, "Temperature programmed dehydration of amorphous calcium phosphate", *J. Collod. Inter. Sci.*, **47** (1974) 483–489.
18. R.Z. LeGeros, G. Bonel, R. LeGeros, "Types of "$H_2O$" in human enamel and in precipitated apatites", *Calcif. Tissue Res.*, **26** (1978) 111–118.
19. *The Chemical Encyclopedic Vocabulary*, I.L. Knunyanc, editor, Soviet Encyclopedia Press, Moscow 1983.
20. N.W. Wikholm, R.A. Beebe, J.S. Kittelberger, "Kinetics of the conversion of monetite to calcium pyrophosphate", *J. Phys. Chem.*, **79** (1975) 853–856.
21. A. Lebugle, E. Zahidi, G. Bonel, "Effect of structure and composition on the thermal decomposition of calcium phosphates (Ca/P = 1.33)", *React. Solids*, **2** (1986) 151–161.
22. B.O. Fowler, E.C. Moreno, W.E. Brown, "Infra-red spectra of hydroxyapatite, octacalcium phosphate and pyrolysed octacalcium phosphate", *Arch. Oral. Biol.*, **11** (1966) 477–492.
23. Z. Zyman, D. Rokhmistrov, V. Glushko, "Structural changes in precipitates and cell model for the conversion of amorphous calcium phosphate to hydroxyapatite during the initial stage of precipitation", *J. Cryst. Growth*, **353** (2012) 5–11.
24. R.A. van Santen, "The Ostwald step rule", *J. Phys. Chem.*, **88** (1984) 5768–5769.
25. S. Raynaud, E. Champion, D. Bernache-Assolant, "Calcium phosphate apatites with variable Ca/P atomic ratio. II. Calcination and sintering", *Biomaterials*, **12** (2002) 1073–1080.
26. E. Champion, "Sintering of CaP bioceramics", *Acta Biomater.*, **9** (2013) 5855–5875.
27. S.V. Dorozhkin, "Bioceramics of calcium orthophosphates", *Biomaterials*, **31** (2010) 1465–1485.